SPECTROSCOPIC METHODOLOGY – Full Paper

Magnetic Resonance in Medicine 66:1209–1217 (2011)

Volume Localized Shift Selective ^{13}C Spectroscopy Using Pulsed Rotating Frame Transfer Sequences With Windows (PRAWN)

Abhishek Banerjee and N. Chandrakumar*

Some novel techniques for volume localized, chemical shift selective ^{13}C spectroscopy are described in this work. These techniques are based on rotating frame *J* cross polarization and are reported for both direct and indirect modes of ^{13}C detection. The performance of two selective mixing sequences, viz., pulsed rotating frame transfer sequences with windows (PRAWN) and PRAWN-π has been studied systematically with different liquid and gel phantoms. Two different front-end modules are used for volume localization, viz., point resolved spectroscopy (PRESS) and localized distortionless enhancement by polarization transfer (LODEPT). It is shown experimentally that both the selective *J* cross polarization sequences can operate efficiently with very low radiofrequency duty cycle; further, they have considerable tolerance to Hartmann-Hahn mismatch. A simple theoretical analysis is also presented to understand *J* cross-polarization dynamics at low RF field amplitudes. Finally, the performance of LODEPT-PRAWN-π is demonstrated for the selective detection of saturated fat in pigeon egg in indirect detection mode. Magn Reson Med 66:1209–1217, 2011. ©2011 Wiley Periodicals, Inc.

Key words: rotating frame coherence transfer; shift selective volume localized ^{13}C magnetic resonance spectroscopy; PRAWN; PRAWN-π; low RF duty cycle; Hartmann-Hahn mismatch tolerance; direct detection; indirect detection; PRESS; LODEPT

^{13}C nuclear magnetic resonance spectroscopy is a powerful tool to study metabolic events in living organisms (1–3). The advantage of this technique is that one can get very high spectral resolution (less crowding of peaks compared to proton nuclear magnetic resonance); however, this is countered by low natural abundance and poor sensitivity, which makes ^{13}C nuclear magnetic resonance (or magnetic resonance spectroscopy) methodology much more challenging than ^{1}H and ^{31}P magnetic resonance spectroscopy. Heteronuclear polarization transfer (PT) (4,5) from abundant spins such as ^{1}H provides a way to enhance the sensitivity of ^{13}C detection. The sensitivity of ^{13}C spectroscopy can be further improved by indirect detection, i.e., selective detection of ^{1}H spins that are coupled to ^{13}C. Some PT studies have been reported in the literature, based primarily on laboratory frame PT protocols (6–12). Among them, the most frequently used sequences are based on distortionless enhancement by polarization transfer (DEPT) (13) and insensitive nuclei enhanced by polarization transfer (INEPT) (14), e.g., localized DEPT (LODEPT) and localized INEPT (LINEPT) (15), and their semi-adiabatic versions (11). Heteronuclear *J* cross polarization (*J*CP) using spin-locking radiofrequency (RF) fields (4) is an important technique for many solid state and liquid state nuclear magnetic resonance experiments to enhance the sensitivity of detection of rare nuclei; however, this technique is not widely used for in vivo experiments. The application of rotating frame PT for ^{13}C localized spectroscopy and for ^{13}C editing has been reported in a series of papers by Kimmich and coworkers (16–18), using the MOIST mixing sequence (19,20) or adiabatic RF fields (21). One technique involves "forward" and "reverse" PT under spin lock conditions, which typically result in reduced motion artifacts. The pulse sequence (CYCLCROP-LOSY) for direct ^{13}C detection comprises PT in three slice selection steps from ^{1}H to ^{13}C, back to ^{1}H and finally once again to ^{13}C. A few studies have been made using *J* cross-polarization for the enhancement of ^{13}C signals in in vivo experiments (22–24). These studies are based on *J* cross-polarization using "narrowband" (~900 Hz) isotropic mixing, such as with WALTZ-4 pulse trains, implemented on a clinical MRI system. Very often, however, in in vivo studies (23,24), interest is focused on a specific metabolite or two. We have, therefore, decided to address this requirement by designing volume localized, chemical shift selective ^{13}C spectroscopy protocols in the rotating frame.

In particular, the objective of this work is to investigate the potential, for volume localized shift selective ^{13}C spectroscopy, of selective *J* cross-polarization using two known mixing sequences, viz., pulsed rotating frame transfer sequences with windows (PRAWN) and its variant PRAWN-π (25). These mixing sequences have low RF power deposition as well as high tolerance to Hartmann-Hahn mismatch and have earlier been used for indirect ^{13}C imaging applications (26,27). We combine these mixing sequences with standard volume localization modules such as point resolved spectroscopy (PRESS) for direct or indirect detection and LODEPT for the indirect detection mode of the present experiment. We demonstrate different aspects of our volume localized selective sequences with theoretical studies and experiments. We also demonstrate the performance of one of these sequences for selective

Department of Chemistry, Indian Institute of Technolog-Madras, Chennai, Tamil Nadu, India.

Grant sponsors: CSIR (Senior Research Fellowship), Indian Institute of Technology-Madras (Research Assistantship), DST (MRM System).

*Correspondence to: N. Chandrakumar, Ph.D., Department of Chemistry, Indian Institute of Technology-Madras, I.I.T. Post Office, Chennai, Tamil Nadu 600036, India. E-mail: nckumar@iitm.ac.in or chandrakumar.iitm@gmail.com

Received 24 August 2010; revised 17 January 2011; accepted 15 February 2011.

DOI 10.1002/mrm.22915

Published online 5 April 2011 in Wiley Online Library (wileyonlinelibrary.com).

detection of saturated fat in a biological sample, viz., pigeon egg.

THEORY

The basic PRAWN sequence (25) consists of a series of RF-pulses with constant flip angle, phase, and interpulse delay; the PRAWN-π sequence is similar to PRAWN, but with an additional π pulse issued in the middle of the sequence, in phase quadrature to the spin-lock pulses as shown in Fig. 1. A detailed theoretical study and the working principle of PRAWN and PRAWN-π may be found elsewhere (25). Here, we recall that the optimum mixing time for AX, AX_2, and AX_3 systems under perfect Hartmann-Hahn match is given as $(2\pi/J)$, $(0.707)(2\pi/J)$ and $(0.61)(2\pi/J)$, respectively, J being the scalar coupling constant expressed in rad s^{-1}. The sequence has several advantages including efficient transfer at very low RF duty cycles, and considerable tolerance to Hartmann-Hahn mismatch, while retaining chemical shift selectivity: all of which are significant practical issues in all in vivo experiments. The tolerance to mismatch (expressed in units of RF amplitude in frequency units) of the basic mixing sequence PRAWN can be related to that of (continuous wave) CW-JCP, scaled up by the inverse of the duty cycle factor. Here, we include an analysis of the sequence applied to an AX system, to explore the efficiency of magnetization transfer under very low RF field amplitudes and report experimental verification of the predictions (28,29).

For simplicity, a heteronuclear two spin-1/2 system IS is considered, in which the I spin is coupled to the S spin through a scalar coupling J rad s^{-1}, and both spins are irradiated on resonance with RF-fields along the x-axes of the doubly rotating frame with respective amplitudes ω_{1I} and ω_{1S} (generically, ω_1). The Hamiltonian in the doubly rotating frame is then given by:

$$H_{\mathrm{DRF}} = \omega_{1I} I_x + \omega_{1s} S_x + J I_z S_z \qquad [1]$$

Under the condition of Hartmann-Hahn match, i.e., with $\omega_{1I} = \omega_{1S} = \omega$, Eq. 1 is modified to:

$$H_{\mathrm{DRF}} = \omega(I_x + S_x) + J I_z S_z \qquad [2]$$

The above Hamiltonian may be expressed in the synchronized doubly rotating frame as

$$H_{\mathrm{SDRF}} = \frac{J}{2}\left(I_z S_z + I_y S_y\right) \qquad [3]$$

Equation 3 is valid only when the RF amplitude ω is significantly larger than the heteronuclear coupling J, permitting truncation of the nonsecular effects of the latter in the synchronized doubly rotating frame. If ω is not significantly larger than J, being instead of the order of J, or even smaller than J, then Eq. 3 fails to model the JCP process because it is independent of ω. To model the effect of weak, Hartmann-Hahn matched RF fields, therefore, we treat the spin system evolution as governed by the Hamiltonian of Eq. 2 in the doubly rotating frame. The evolution of an initial density matrix I_x under

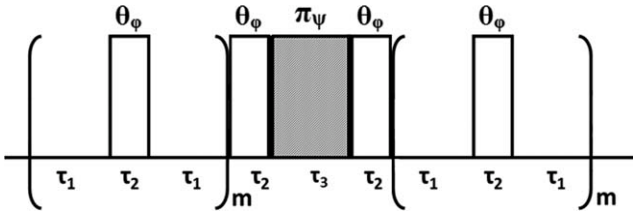

FIG. 1. Basic PRAWN-π sequence. If $n = 2(m + 1)$ is the number of pulses with flip angle θ, the total rotation is given by $n\theta = 2\pi$ and mixing time $= 2m(2\tau_1 + \tau_2) + 2\tau_2 + \tau_3$. The phase difference $(\varphi - \psi)$ between the θ and π pulses is $\pm\pi/2$.

the Hamiltonian of Eq. 1 may be computed using the standard Baker-Campbell-Hausdorff expansion. The successive nested commutators that occur in the BCH expansion may be readily fitted to sine and cosine functions. We may thus adopt a simple procedure to grasp the JCP dynamics at any arbitrary RF field strength. Let the time evolution of the initial density operator be expressed as:

$$1 + a(1 - \cos(f_1 t)) + b(1 - \cos(f_2 t)) + c(1 - \cos(f_3 t)) + \cdots \qquad [4]$$

On the other hand, the time evolution of the density matrix components generated in course of time is given by:

$$a_1(1 - \cos(f_1 t)) + b_1(1 - \cos(f_2 t)) + c_1(1 - \cos(f_3 t)) + d_1(\sin(f_4 t)) + \cdots \qquad [5]$$

Here f_1, f_2, f_3, f_4, ... are the angular frequencies of evolution, which may be obtained by diagonalizing the matrix representation of the Hamiltonian of Eq. 1, then taking differences of pairs of eigenvalues; a, b, c, a_1, b_1, c_1, d_1, etc. are amplitudes of the various oscillatory terms. To determine the amplitudes, a set of simultaneous equations is solved, with the coefficients of each operator being obtained from the successive nested commutators of the BCH expansion. This set of coefficients of each operator is then equated to the corresponding terms in the series expansion of the appropriate time function. We have used MATHEMATICA to solve these simultaneous equations algebraically. For the two spin-1/2 system described by the Hamiltonian of Eq. 2, I_x (generated by a $\pi/2$ pulse issued in the y-direction on the I spins, that are initially in thermal equilibrium) is converted into in-phase S_x under Hartmann-Hahn match, with the following time dependence and amplitude:

$$I_x \rightarrow \left[\tfrac{1}{2}(1 - \cos(f_1 t)) - \frac{J^2}{(2J^2 + 32\omega^2)}(1 - \cos(f_2 t))\right] S_x \qquad [6]$$

In this case, $f_1 = J/2$ and $f_2 = \sqrt{J^2 + 16\,\omega^2}/2$. The above closed analytical solution can be useful to study the JCP dynamics for any arbitrary ratio of ω/J. Figure 2 shows the amplitude of S_x generated as a function of Jt for three different values of RF amplitude, ω.

From Fig. 2, it is clear that the optimum mixing time corresponding to the first maximum is not a monotonically decreasing function of ω. At $\omega = J/2$, there is a decrease in optimum mixing time by 4% as compared with the situation for $\omega = J$. However, the optimal

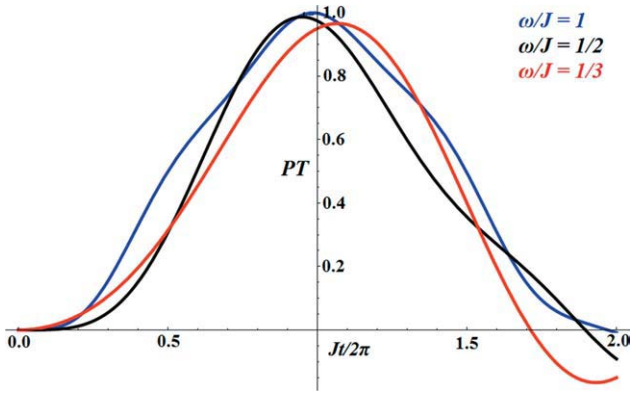

FIG. 2. Efficiency of cross polarization of PRAWN sequence at different RF power amplitudes, plotted as a function of $Jt/2\pi$. The figure clearly shows that the almost full transfer is observed with one-fourth of the RF power at $\omega = J/2$ as compared with the situation with $\omega = J$.

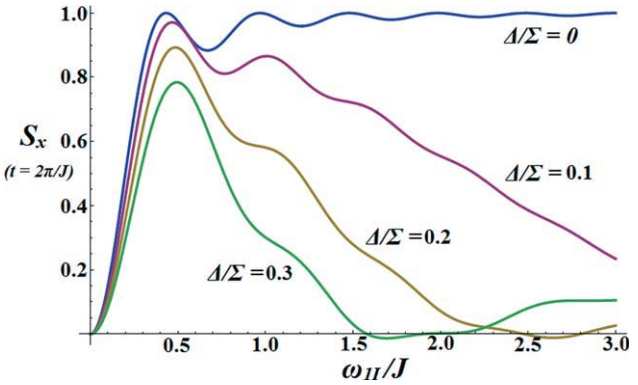

FIG. 3. The amplitude of S_x magnetization as a function of ω_{1I}/J at different mismatch levels, generated using Eq. 7. Here $\Delta = (\omega_{1I} - \omega_{1S})/J$ and $\Sigma = (\omega_{1I} + \omega_{1S})/J$.

mixing time increases when $\omega = J/3$. It is interesting to note that at $\omega = J/2$ almost full transfer is observed with one-half the RF amplitude (i.e., one-fourth of the RF power) as compared with the situation for $\omega = J$.

Under conditions of Hartmann-Hahn mismatch on-resonance, on the other hand, the amplitude of S_x magnetization resulting from I_x is given by:

$$I_x \rightarrow \left[\frac{1}{2\left(1+4\Delta^2\right)}\left(1-\cos\left(\frac{\sqrt{1+4\Delta^2}}{2}Jt\right)\right) - \frac{1}{2\left(1+4\Sigma^2\right)}\left(1-\cos\left(\frac{\sqrt{1+4\Sigma^2}}{2}Jt\right)\right)\right]S_x \qquad (7)$$

Here, $\Delta = (\omega_{1I} - \omega_{1S})/J$ and $\sum = (\omega_{1I} + \omega_{1S})/J$. In Fig. 3, the amplitude of I_x transferred to S_x at a time $t = 2\pi/J$ is plotted as a function of ω_{1I}/J with different ratios of $\Delta/\sum$ according to Eq. 7. As expected, the efficiency of the transfer decreases with increasing mismatch. It is seen from the figure that for a mixing time $t = 2\pi/J$ and $\omega_{1I} \sim J/2$, on-resonance Hartmann-Hahn mismatch parameter value of $\Delta = 1/6$ leads to a drop in coherence transfer efficiency of around 10% (cf. plot for $\Delta/\Sigma = 0.2$).

METHODS

To combine volume localization with selective J cross-polarization, we have developed the PRESS-PRAWN and PRESS-PRAWN-π sequences for direct detection, and the PRESS-[PRAWN-π]^2 and LODEPT-PRAWN-π sequences for indirect detection. In all these cases, the front-ends, viz., PRESS (30) or LODEPT achieve volume localization, whereas the PRAWN-based module(s) achieve(s) selective coherence transfer under low-power pulsed spin lock.

All the experiments were performed on a Bruker 500 MHz WB US$^+$ MRM system with a 38 mm $^1H/^{13}C$ double-tuned resonator. We have tested our sequence on AX, AX_2, and AX_3 spin systems with a variety of samples. For direct detection tests, we used two phantom samples: pure $CHCl_3$ (J_{CH} = 210 Hz) and ethanol ($J_{CH}(CH_2)$ = 141 Hz, $J_{CH}(CH_3)$ = 126 Hz). To check the performance of PRAWN at low ω_1, we used 100 mM lactic acid (J_{CH} = 220 Hz) in 1% agar gel, and 100 mM ethanol in 1% agar gel. Finally, indirect detection with PRAWN-π was performed on a pigeon egg for selective detection of saturated fat in egg yolk.

Direct Detection

For volume localized direct detection of ^{13}C, PRAWN and PRAWN-π were implemented with the PRESS localization technique, as shown in Fig. 4. The phase of the first π/2 pulse in PRESS is in quadrature to the phase of the spin lock sequence. The mixing sequence PRAWN consists of 18 π/9 pulses, each of 50 μs, with 18 constant delays (adjusted according to the optimal contact time for each of the spin systems). In the PRAWN-π sequence, the phase of the π pulse is in quadrature to the rest of the PRAWN sequence. Both sequences are terminated with a hard π/2 pulse on ^1H to minimize phase and multiplet anomalies.

Comparison of PRESS-PRAWN-π With LODEPT and PRESS-CW-π-JCP

For comparison, we have also performed the corresponding LODEPT and CW-*J*CP experiments. In the LODEPT sequence, the delay ($\Delta = 1/(2J)$) was adjusted according

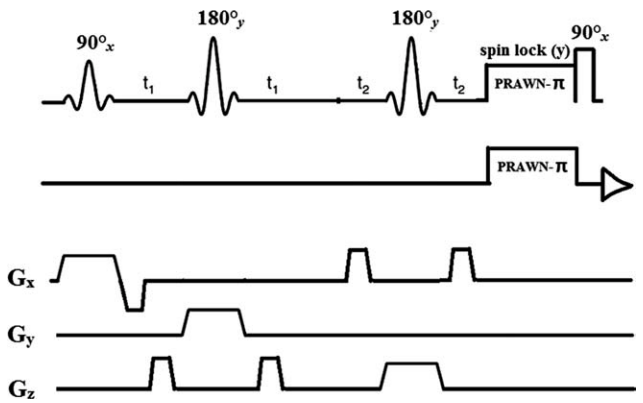

FIG. 4. PRAWN-π sequence implemented with PRESS as front-end, for shift selective, volume localized direct detection of ^{13}C nuclei. The PRAWN-π sequence consists of 18-segment PRAWN pulse train with total rotation 360° (flip angle and duration of each pulse was π/9 and 50 μs, respectively).

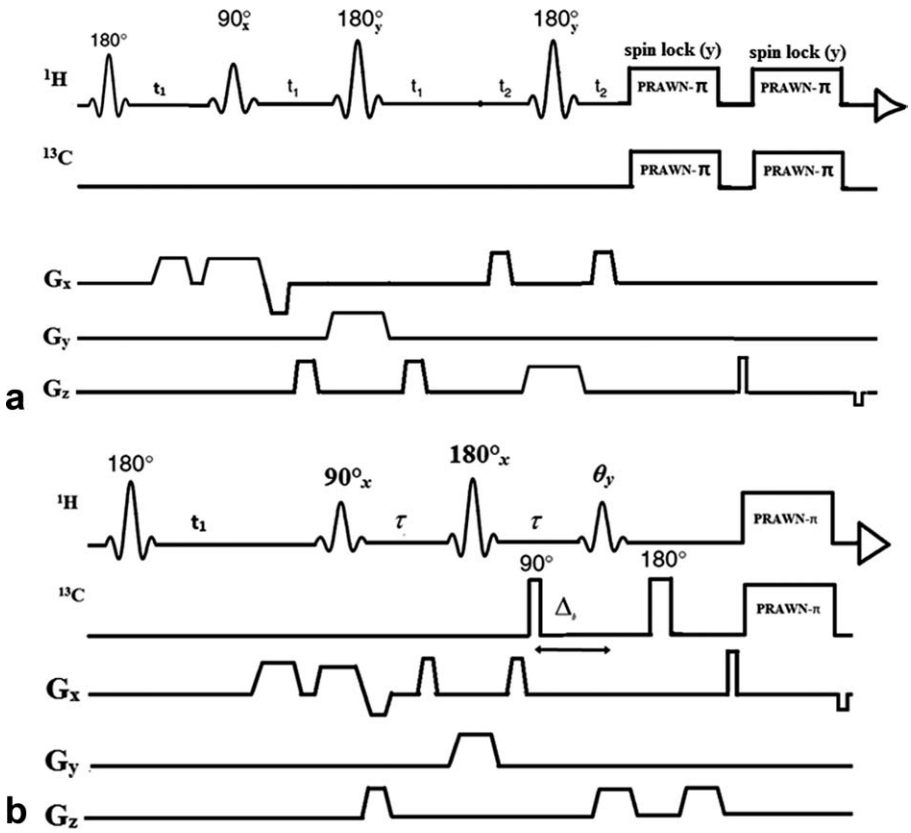

FIG. 5. Shift selective volume localized indirect detection of ^{13}C using: (**a**) PRESS-[PRAWN-π]^2, cyclic polarization transfer $^1H \rightarrow {}^{13}C \rightarrow {}^1H$ being performed using two PRAWN-π mixing blocks; and (**b**) LODEPT-PRAWN-π, volume localization together with $^1H \rightarrow {}^{13}C$ polarization transfer being performed with LODEPT the subsequent $^{13}C \rightarrow {}^1H$ transfer being performed using PRAWN-π. Water suppression was performed with a simple inversion recovery (zero crossing) scheme.

to the coupling of AX, AX_2, and AX_3 spin systems, and the flip angle of the last proton pulse was set to π/4. It may be noted that this choice of flip angle is optimal for the AX_2 group and within 9% of the optimum for the AX_3 group, but is 29% below the optimum for the AX system; it is a compromise setting for different spin systems. Selective, mismatch compensated CW-*J*CP experiments were also performed with a similar approach as in PRESS-PRAWN-π, mismatch being compensated by introducing a π pulse with quadrature phase in the middle of the CW spin lock pulse; we may term this as PRESS-CW-π-*J*CP. A 64 mm^3 voxel was excited in all three experiments, viz., LODEPT, PRESS-PRAWN-π, and PRESS-CW-π-*J*CP, with three selective 1 ms sinc pulses; all other relevant parameters were kept constant.

Low Power Performance

The average RF amplitude ω_{1av} during a windowed sequence such as PRAWN may be calculated from the expression: $\omega_{1av} = \omega_{1p} \times$ (duty cycle factor). Here, ω_{1p} is the RF amplitude of the individual PRAWN pulses in the train; the duty cycle factor, i.e., the ratio of RF on-time to total cycle duration, is expressed as a fraction of 1. The efficiency of cross-polarization of PRAWN at very low average RF field amplitude (ω_{1av}) was benchmarked experimentally. We have implemented PRAWN with a PRESS front-end for volume localization. For AX, AX_2, and AX_3 systems, two sets of experiments were performed; in one, the average RF amplitude was set to ~200 Hz, whereas this was reduced to ~100 Hz in a second set of experiments. All experiments were performed with the two gel samples mentioned above.

Mismatch Tolerance

We have tested the Hartmann-Hahn mismatch tolerance of PRESS-PRAWN, PRESS-CW-*J*CP, and their variants with a mismatch compensating π pulse. A set of experiments was performed with a liquid $CHCl_3$ sample without ^1H decoupling. Both hetero spins were irradiated on resonance with an 18-segment PRAWN pulse train with total rotation 360°. Mixing time for PT was set to 4.761 ms (J = 210 Hz). ^1H channel power level was varied in a range of ±5 dB, in 1 dB steps around 5.44 dB (π/9 pulse of 50 μs).

Indirect Detection

Shift selective volume localized ^{13}C indirect detection was implemented in a "cyclic" fashion, two different pulse sequences that we have designed for this purpose being shown in Fig. 5a,b.

For volume localized indirect detection of ^{13}C, PRAWN-π was implemented with the PRESS localization technique, as shown in Fig. 5a. All three pulses in the PRESS module are selective sinc pulses of 1 ms duration. After volume localization, polarization is transferred from ^1H to ^{13}C and then back to ^1H with two PRAWN-π blocks in succession. A pair of gradients in a 4:−1 ratio is used to suppress signals from ^1H bound to ^{12}C. Water suppression is performed with a selective π pulse on the water resonance, followed by a delay t_1 to allow for the zero-crossing of the water signal. An additional gradient may be used to dephase residual transverse magnetization from water. Other water suppression techniques such as chemical shift selective excitation (CHESS) (31) or variable power and optimized relaxation

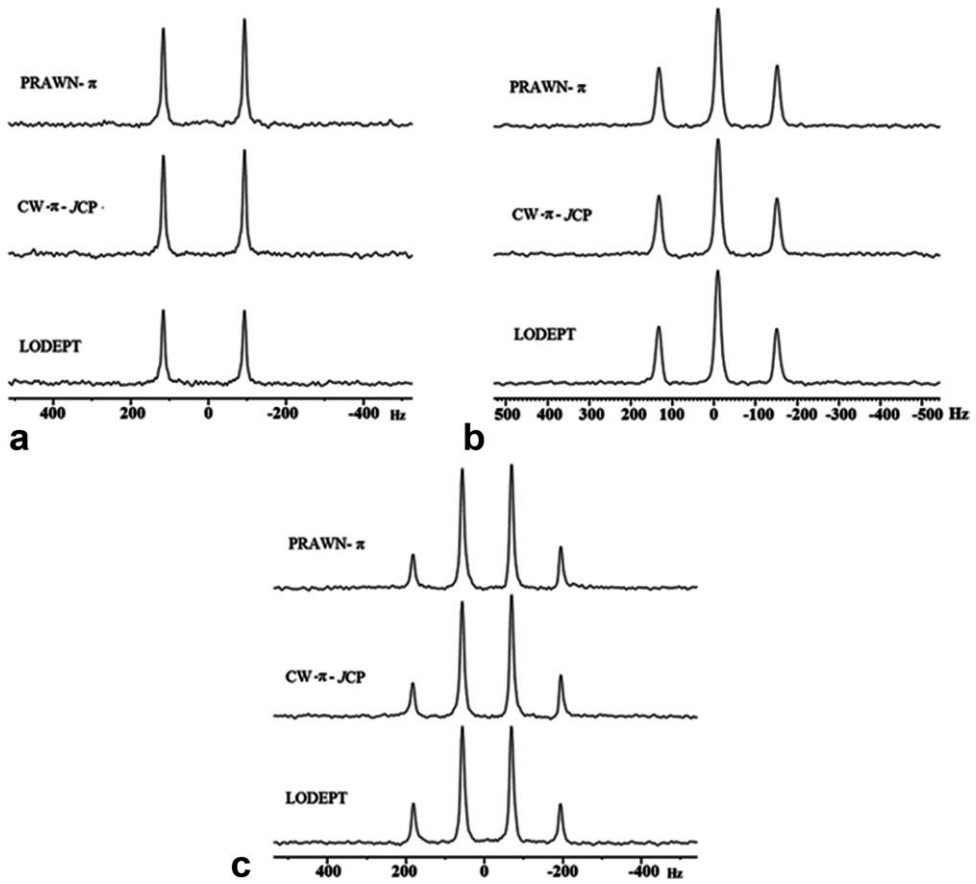

FIG. 6. Comparisons of PRESS-PRAWN-π with LODEPT and PRESS-CW-π-*J*CP. Lower trace: LODEPT, middle trace: CW-π-*J*CP, and upper trace: PRAWN-π. Both CW-π-*J*CP and PRAWN-π were implemented with a PRESS front-end. **a**: —CH of $CHCl_3$, (**b**) —CH_2 of ethanol, and (**c**) —CH_3 of ethanol.

(VAPOR) (32) may be used as well. The sequence was tested on pure $CHCl_3$ sample.

Figure 5b shows the LODEPT-PRAWN-π sequence. Water suppression is performed in the same manner as described above. PT from ^1H to ^{13}C with volume localization is then performed with a LODEPT module. All three pulses on the ^1H channel in LODEPT are selective sinc pulses of 1 ms duration. ^{13}C magnetization is again transferred back to ^1H with the PRAWN-π sequence, followed by detection. A pair of gradients in a 4:−1 ratio is used to suppress signals from ^1H bound to ^{12}C. The selectivity and water suppression of this sequence have been tested with a gel sample of 100 mM ethanol. We have used this sequence for selective detection of saturated fat in pigeon egg and have also compared the performance of this sequence with PRAWN-π replaced by a CW-π-*J*CP module. It seems to us that LODEPT-PRAWN-π is to be preferred over PRESS-[PRAWN-π]^2, because of the extended duration and additional RF pulsing involved in the latter.

RESULTS

Direct Detection

Comparison of PRESS-PRAWN-π With LODEPT and PRESS-CW-π-JCP

We have compared PRESS-PRAWN-π with LODEPT and PRESS-CW-π-*J*CP for all three spin systems (AX, AX_2, and AX_3). Figure 6 shows the localized ^{13}C spectrum acquired in direct detection mode. The average value of ω_1 was maintained constant, in comparing PRESS-PRAWN-π with PRESS-CW-π-*J*CP. Phase distortion and multiplet anomalies are common issues in heteronuclear cross-polarization experiments, especially for AX_2 and AX_3 spin systems. In our experiments, these anomalies were suppressed by the last π/2 termination pulse (after the spin-lock period), issued on the proton channel in phase quadrature with the spin lock sequence.

The sensitivity of both PRESS-PRAWN-π and PRESS-CW-π-*J*CP was superior to LODEPT for AX and AX_2 spin systems, whereas it was comparable for the AX_3 spin system. Total gain in signal intensity relative to LODEPT for AX and AX_2 spin systems was 25% and 10%, respectively.

Effect of Weak RF Fields

In the "Theory" section, we have pointed out that the PRAWN sequence has the ability to work at very low RF field amplitude (ω_{1av}). Figure 7a–c (upper trace in each case) was obtained on AX, AX_2, and AX_3 systems with $\omega_{1av}/2\pi$ of 218 Hz, 196 Hz, and 204 Hz, respectively, whereas the lower trace of Fig. 7a–c was obtained with RF field amplitude equal to 109 Hz, 98 Hz, and 102 Hz, respectively.

In all cases, the transfer efficiency at the lower RF amplitude is seen to be essentially identical to that at the higher RF amplitude. There is a slight gain in intensities in the outer multiplet components of AX_2 and AX_3 spin systems at low ω_{1av}.

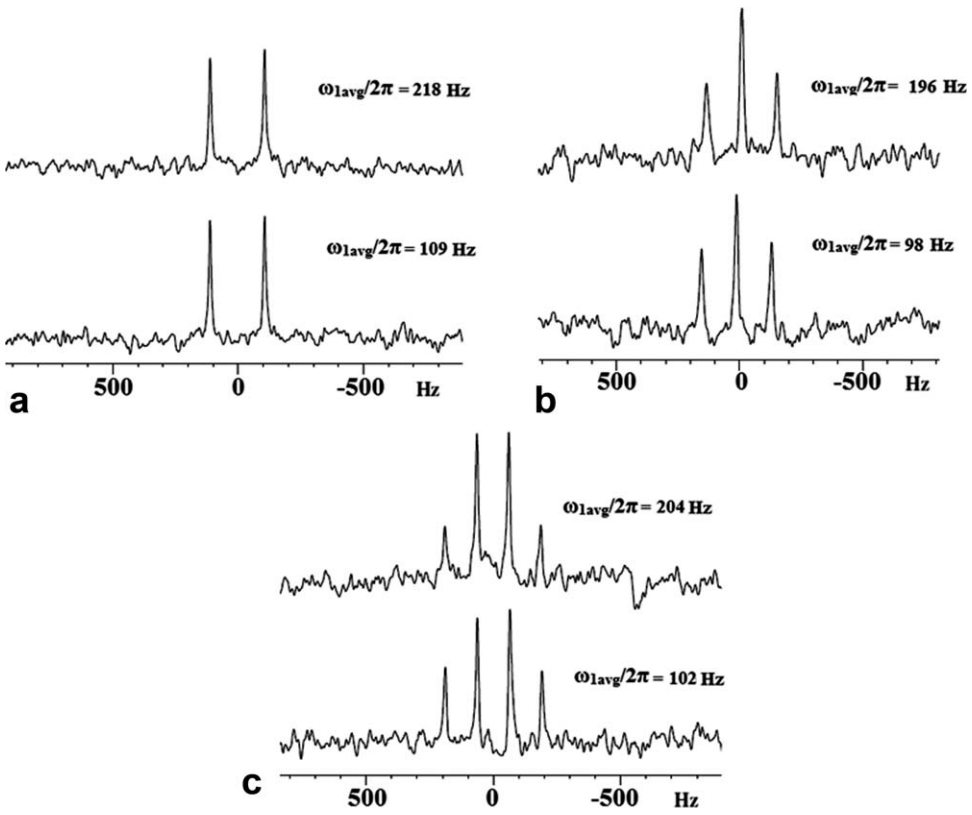

FIG. 7. Performance of PRESS-PRAWN at low RF field amplitude. **a**: —CH of 100 mM lactic acid in 1% agar gel. **b**,**c**: —CH_2 and —CH_3 of 100 mM ethanol in 1% agar gel, respectively. The spectra of the lower traces are obtained with the lower *J*CP RF amplitudes inscribed in the figure, whereas the upper traces are obtained with the higher RF amplitudes inscribed.

Effect of Hartmann-Hahn Mismatch

We have tested the Hartmann-Hahn mismatch tolerance of both PRESS-PRAWN and PRESS-PRAWN-π sequences. A set of experiments was performed with a $CHCl_3$ sample without ^{1}H decoupling. Both spins were irradiated on-resonance with an 18-segment PRAWN pulse train with total rotation 360°. The mixing time for PT was set to 4.761 ms ($J = 210$ Hz). ^{1}H channel power level was varied around 5.44 dB (50 μs π/9 pulse) in a range of ±5 dB in 1 dB steps. Figure 8 shows the variation of the ^{13}C signal with ^{1}H power level for three different pulse sequences; note that 5.44 dB has been denoted as 0 in the figure.

All experiments were performed with a PRESS front-end. As noted earlier, the tolerance range (expressed in Hz) of the PRAWN mixing sequence to Hartmann-Hahn mismatch is related to that of CW-*J*CP for the same $\omega_{1av}/2\pi$, scaled however by the inverse duty cycle factor. The PRAWN-π and CW-π-*J*CP mixing sequences exhibit a pronounced increase in tolerance to Hartmann-Hahn mismatch, over a range of ±4 dB, the performance of PRAWN-π being nominally better than the CW-π-*J*CP experiment, possibly because of a degree of freedom from transmitter droop effects and probe heating effects.

Suppression of water and the ^{12}C—^{1}H signal is clearly satisfactory. The —CH_2 spin system of ethanol shows some extra enhancement of signal, attributable to the nuclear Overhauser effect.

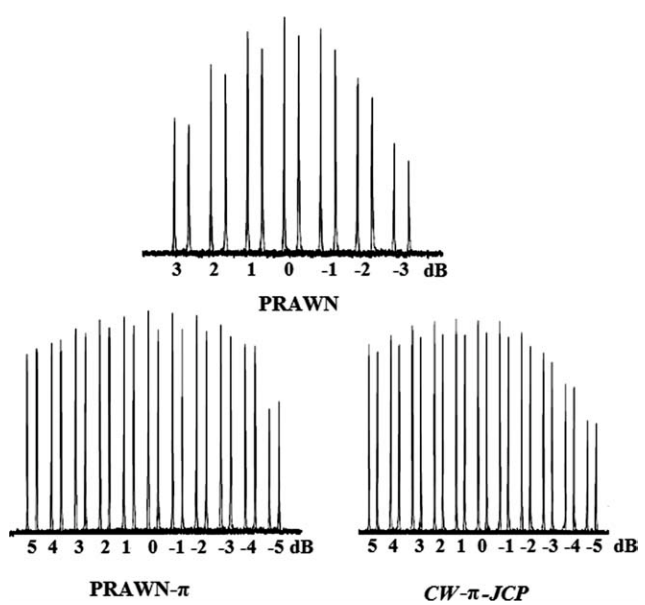

FIG. 8. Hartmann-Hahn tolerance of: (Top) PRAWN, (bottom left) PRAWN-π, and (bottom right) CW-π-*J*CP. All three sequences were implemented with PRESS as front-end. Signal obtained with a pure $CHCl_3$ phantom. ^{1}H channel power level was varied from 5.44 dB (denoted 0 in the figure) in a range of ±5 dB in 1 dB steps, keeping the power level on the ^{13}C channel constant.

Indirect Detection

Figure 9 shows the 100 mM ethanol spectrum in 1% agar gel, acquired with LODEPT-PRAWN-π. The water signal was suppressed with a selective 180° sinc pulse followed by a delay of 0.9 s.

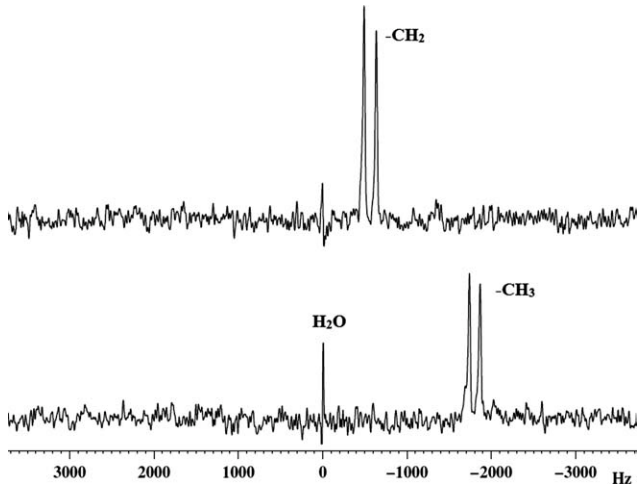

FIG. 9. Spectrum of 100 mM ethanol, obtained with LODEPT-PRAWN-π sequence. Lower trace: —CH_3 of ethanol; upper trace: —CH_2 of ethanol. Water signal was suppressed with a selective 10 ms 180° sinc pulse followed by a delay of 0.9 s.

Working with $CHCl_3$, the performance of PRESS-[PRAWN-π]^2 and LODEPT-PRAWN-π were equivalent; the former sequence was not pursued, however, for the reasons discussed earlier.

Application to Pigeon Egg

Finally, the LODEPT-PRAWN-π sequence was used for selective detection of saturated fat in a chosen voxel in a pigeon egg. The voxel of interest was identified by standard multislice gradient echo imaging. Multislice images were obtained in all three tomographic orientations, namely, axial, sagittal, and coronal. Figure 10a shows a coronal gradient echo image of pigeon egg, acquired with pulse repetition time 200 ms, echo time 4.1 ms, slice thickness 2 mm, and field of view 6 cm. All images clearly show two major compartments of egg, namely, protein-rich egg white (albumin) and lipid-rich yolk. Standard ^1H PRESS spectra were obtained from egg yolk and an example is shown in Fig. 10b. While the resonances at 1.2 and 0.8 ppm are assigned to CH_2 and CH_3 moieties of yolk lipid, the resonances at 2.15 and 1.9 ppm could be from the egg yolk fatty acid. The residual peak at 4.8 ppm is due to water. The lipid content is almost zero in egg white as demonstrated by the localized ^1H spectrum obtained from egg white (data not shown here).

Figure 11a shows the proton detected volume localized ^{13}C spectrum of saturated fat from a voxel chosen in the egg yolk region of pigeon egg using LODEPT-PRAWN-π (lower trace) and LODEPT-CW-π-*J*CP (upper trace). Figure 11b demonstrates the voxel selection capability of the LODEPT-PRAWN-π sequence, displaying the noise trace (lower trace) that results in this chemical shift region from the egg white voxel. In each case, the saturated fat signal at 1.2 ppm was excited on-resonance. Both spectra were acquired from a $8 \times 8 \times 8$ mm^3 voxel with a *J*CP mixing time 5.6 ms (0.707/*J*, $J = 126$ Hz), the number of scans being 512; $\omega_{1av}/2\pi$ for cross polarization was set to 174 Hz. The proton detected ^{13}C spectrum of the methylene group yields a doublet at 1.2 ppm. Suppression of the water signal is clearly of acceptable quality in both spectra, especially so in the PRAWN-π spectrum. More important, we have 35% more signal intensity with LODEPT-PRAWN-π than in the corresponding CW-π experiment. An attempt to use the PRAWN mixing sequence at lower ω_1 amplitude was, however, unsuccessful with the egg sample due to the very short T_2^* of the saturated fat signal (^1H line width: 97 Hz).

DISCUSSION

The results of these studies demonstrate efficient shift selective cross-polarization between ^1H and ^{13}C using the PRAWN and PRAWN-π mixing sequences for volume localized applications. Both sequences have been used satisfactorily on AX, AX_2, and AX_3 spin systems for both direct and indirect detection of ^{13}C spins. PRAWN and PRAWN-π sequences have been implemented with a PRESS front-end for ^{13}C direct detection, although they may be used with other localization techniques as well, such as ISIS (33). The most attractive features of both sequences are selectivity, efficient transfer

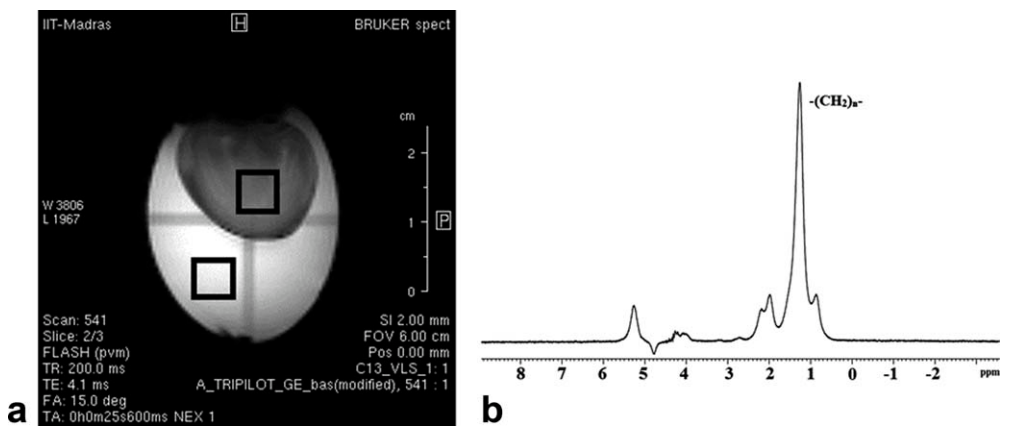

FIG. 10. **a**: A coronal gradient echo image of pigeon egg, acquired with pulse repetition time 200 ms, echo time 4.1 ms, slice thickness 2 mm, and field of view 6 cm. **b**: Standard water suppressed ^1H PRESS spectrum was obtained from egg yolk with pulse repetition time 1500 ms, echo time 16 ms, NS 4, and $8 \times 8 \times 8$ mm^3 voxel.

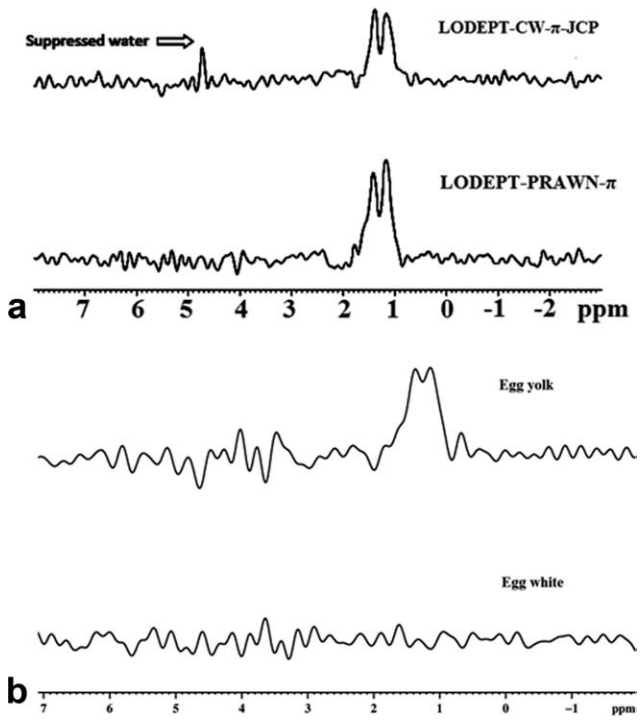

FIG. 11. Indirect selective detection of saturated fat in Pigeon egg using the LODEPT-CW-π-*J*CP and LODEPT-PRAWN-π sequences. **a**: Upper trace: LODEPT-CW-π-*J*CP; lower trace: LODEPT-PRAWN-π. **b**: LODEPT-PRAWN-π applied to a voxel in egg yolk (upper trace) and in egg white (lower trace). All spectra were acquired from a $8 \times 8 \times 8$ mm^3 voxel with a *J*CP mixing time 5.6 ms (0.707/*J*, $J = 126$ Hz), the number of scans being 512 with a LODEPT front-end.

at very low RF field amplitudes, very low RF duty cycle, and considerable tolerance to Hartmann-Hahn mismatch. In contrast, most of the previously reported methods (17,22–24) were semi-selective in nature and the average RF amplitude used for cross polarization was in the range 700–1200 Hz, whereas it is only ~200 Hz or even less in the present studies. The mixing sequence PRAWN exhibits useful tolerance to Hartmann-Hahn mismatch. PRAWN-π exhibits a still wider tolerance range to Hartmann-Hahn mismatch. This is due to the fact that the π pulse rephases the in-phase and anti-phase antisymmetric components of the density matrix (25). It has been noted (25) that the PRAWN-π sequence compensates Hartmann-Hahn mismatch while retaining the signal dependence on resonance offset in terms of the tilt parameters of the off-resonance spin Hamiltonian; this seems to be an attractive characteristic especially suited for imaging and the volume localized spectral applications in view, as in practice this implies retention of selectivity in PT, while compensating for mismatch, including effects of field drifts which are sensed in proportion to γ.

Indirect detection using LODEPT-PRAWN-π also turns out to be very satisfactory in terms of selectivity and transfer efficiency. The superior performance of PRAWN-π compared with CW-π-*J*CP in inhomogeneous media is verified by experiments performed with AX, AX_2, and AX_3 spin systems in 1% agar gel (data not shown here) and arises possibly because of a degree of freedom from transmitter droop effects and probe heating effects. This superiority of PRAWN-π is especially relevant in a "real life" situation, as demonstrated on pigeon egg, using a LODEPT front-end followed by the PRAWN-π module for the selective indirect detection of saturated fat in pigeon egg.

CONCLUSIONS

The PRAWN and PRAWN-π mixing sequences for AX, AX_2, and AX_3 spin systems have been used successfully for volume localized ^{13}C spectroscopy, *J* being in the range 120–210 Hz, using average RF amplitudes of the same order. Different aspects of PRAWN have been studied systematically, including the ability of PRAWN to work at very low average RF field amplitudes. The performance of the sequences has been compared with known popular techniques such as LODEPT; it has been found that the new sequences result in improved sensitivity, especially for AX_2 systems. The incorporation of a π pulse in PRAWN results in very high tolerance to Hartmann-Hahn mismatch. This PRAWN-π sequence was successfully implemented with a LODEPT front-end for voxel selection, to achieve shift selective detection of saturated fat in pigeon egg in indirect detection mode. It appears reasonable to conclude that both versions of the PRAWN sequences may be used efficiently in in vivo experiments for shift selective direct and indirect detection of ^{13}C metabolites.

ACKNOWLEDGMENTS

A.B. thanks CSIR and the Indian Institute of Technology, Madras for the grant of a Senior Research Fellowship and of a Research Assistantship, respectively; N.C. thanks DST for grant of the MRM system. The authors also thank Ms. Christy George, Senior Research Fellow, for her kind help with the final version of the manuscript. NC acknowledges with pleasure a Research Co-operation Agreement between Bruker Switzerland and IIT Madras, Chennai, under which the mini-imaging system was kindly made available by M/s Bruker for the Avance II 500 MHz WB US+ system at IIT Madras.

REFERENCES

1. Chance EM, Seeholzer SH, Kobayashi K, Williamson JR. Mathematical analysis of isotope labeling in the citric acid cycle with applications to ^{13}C NMR studies in perfused rat hearts. J Biol Chem 1983; 258:13785–13794.
2. Gruetter R, Adriany G, Cho I-Y, Henry P-G, Lei H, Öz G. Localized *in vivo* ^{13}C NMR spectroscopy of the brain. NMR Biomed 2003;16: 313–338.
3. van Zijl PCM, Rothman D. NMR studies of brain C-13-glucose uptake and metabolism—present status. Magn Reson Imaging 1995;13: 1213–1221.
4. Hartmann SR, Hahn EL. Nuclear double resonance in the rotating frame. Phys Rev 1962;128:2042–2053.
5. Aue WP, Muller S, Seelig J. Localized ^{13}C NMR spectra with enhanced sensitivity obtained by volume-selective excitation. J Magn Reson 1985;61:392–395.
6. Irving MG, Simpson SJ, Brooks WM, Holmes RS, Doddrell DM. Application of the reverse dept polarization-transfer pulse sequence to monitor in vitro and in vivo metabolism of ^{13}C- ethanol by ^{1}H-NMR spectroscopy. Int J Biochem 1985;17:471–478.

7. Knüttel A, Kimmich R, Spohn K-H. Single-scan volume-selective editing of ^{1}H signals for the indirect detection of coupled X nuclei. J Magn Reson 1989;81:570–576.
8. Knüttel A, Kimmich R, Spohn K-H. Indirect ^{13}C tomography and volume-selective spectroscopy via proton NMR. I. Spectroscopic techniques. J Magn Reson 1990;86:526–541.
9. Bomsdorf H, Roschmann P, Wieland J. Sensitivity enhancement in whole-body natural abundance ^{13}C spectroscopy using $^{13}C/^{1}H$ double-resonance techniques at 4 Tesla. Magn Reson Med 1991;22:10–22.
10. Saner M, McKinnon G, Boesiger P. Glycogen detection by *in vivo* ^{13}C NMR: a comparison of proton decoupling and polarization transfer. Magn Reson Med 1992;28:65–73.
11. Henry P-G, Tkáč I, Gruetter R. ^{1}H-localized broadband ^{13}C NMR spectroscopy of the rat brain in vivo at 9.4 T. Magn Reson Med 2003; 50:684–692.
12. Beckmann N, Muller S. Analysis of localized polarization transfer for ^{13}C volume-selective spectroscopy with surface coils. J Magn Reson 1991;93:299–318.
13. Doddrell DM, Pegg DT, Bendall MR. Distortionless enhancement of NMR signals by polarization transfer. J Magn Reson 1982;48: 323–327.
14. Morris GA, Freeman R. Enhancement of nuclear magnetic resonance signals by polarization transfer. J Am Chem Soc 1979;101: 760–762.
15. Watanabe H, Ishihara Y, Okamoto K, Oshio K, Kanamatsu T, Tsukada Y. In vivo 3D localized ^{13}C spectroscopy using modified INEPT and DEPT. J Magn Reson 1998;134:214–222.
16. Köstler H, Kimmich R. Adiabatic *J* cross polarization for localized direct and proton-detected ^{13}C spectroscopy. J Magn Reson B 1993; 102:285–292.
17. Kunze C, Kimmich R. Motion-insensitive localized ^{13}C spectroscopy using cyclic and slice-selective J cross polarization. J Magn Reson B 1994;105:38–44.
18. Kunze C, Kimmich R, Demco DE. Cyclic and slice-selective J cross polarization for heteronuclear editing and localized NMR. J Magn Reson A 1993;101:277–284.
19. Levitt MH, Suter D, Ernst RR. Spin dynamics and thermodynamics in solid-state NMR cross polarization. J Chem Phys 1986;84: 4243–4255.
20. Levitt MH. Heteronuclear cross polarization in liquid-state nuclear magnetic resonance: mismatch compensation and relaxation behaviour. J Chem Phys 1991;94:30–38.
21. Chingas GC, Garroway AN, Moniz WB, Bertrand RD. Adiabatic J cross-polarization in liquids for signal enhancement in NMR. J Am Chem Soc 1980;102:2526–2528.
22. Artemov D, Bhujwalla ZM, Glickson JD. In vivo selective measurement of (1–13C)-glucose metabolism in tumors by heteronuclear cross polarization. Magn Reson Med 1995;33:151–155.
23. Artemov D, Bhujwalla ZM, Maxwell RJ, Griffiths JR, Judson IR, Leach MO, Glickson JD. Pharmacokinetics of the ^{13}C labeled anticancer agent temozolomide detected in vivo by selective cross-polarization transfer. Magn Reson Med 1995;34:338–342.
24. van den Bergh AJ, van den Boogert HJ, Heerschap A. Heteronuclear cross polarization for enhanced sensitivity of in vivo ^{13}C MR spectroscopy on a clinical 1.5 T MR system. J Magn Reson 1998;135:93–98.
25. Chandrakumar N, Kimmich R. PRAWN: mixing sequences for selective heteronuclear *J* cross polarization. J Magn Reson 1999;137:100–107.
26. Spyros A, Chandrakumar N, Heidenreich M, Kimmich, R. Selective determination of elastomer distribution in multicomponent systems using proton-detected ^{13}C imaging. Macromolecules 1998;31: 3021–3029.
27. Heidenreich M, Köckenberger W, Kimmich R, Chandrakumar N, Bowtell R. Investigation of carbohydrate metabolism and transport in castor bean seedlings by cyclic *J* cross polarization imaging and spectroscopy. J Magn Reson 1998;132:109–124.
28. Vijayan V. Selective heteronuclear cross-polarization in scalar coupled spin systems. MSc Dissertation. Madras: IIT; 2002.
29. Chandrakumar N. Rotating frame coherence transfer in solution state NMR. Proc Ind Natl Sci Acad 2004;70A:659–663
30. Bottomley PA. Selective volume method for performing localized NMR spectroscopy. US Patent 4,480,228, 1984.
31. Haase A, Frahm J, Hanicke W, Matthaei D. ^{1}H NMR chemical shift selective (CHESS) imaging. Phys Med Biol 1985;30:341–344.
32. Tkáč I, Starčuk Z, Choi I-Y, Gruetter R. In vivo ^{1}H NMR spectroscopy of rat brain at 1 ms echo time. Magn Reson Med 1999;41:649–656.
33. Ordidge RJ, Connelly A, Lohman JAB. Image-selected *in vivo* spectroscopy (ISIS): a new technique for spatially selective NMR spectroscopy. J Magn Reson 1986;66:283–294.